Chiral Metamaterial Predicted by Granular Micromechanics: Verified with 1D Example Synthesized using Additive Manufacturing

Anil Misra[1*], Nima Nejadsadeghi[2], Michele De Angelo[1,3], Luca Placidi[4]

[1]Civil, Environmental and Architectural Engineering Department,
University of Kansas, 1530 W. 15th Street, Learned Hall, Lawrence, KS 66045-7609.
[2]Mechanical Engineering Department,
University of Kansas, 1530 W. 15th Street, Learned Hall, Lawrence, KS 66045-7609.
[3]Dipartimento di Ingegneria Civile, Edile-Architettura e Ambientale, Università degli Studi dellAquila, Via Giovanni Gronchi 18 - Zona industriale di Pile, 67100 LAquila, Italy
[3]International Telematic University Uninettuno,
C. so Vittorio Emanuele II 39, 00186 Rome, Italy
*corresponding author: Ph: (785) 864-1750, Fax: (785) 864-5631, Email: amisra@ku.edu

Continuum Mechanics and Thermodynamics

Abstract

Granular micromechanics approach (GMA) provides a predictive theory for granular material behavior by connecting the grain-scale interactions to continuum models. Here we have used GMA to predict the closed-form expressions for elastic constants of macro-scale chiral granular metamaterial. It is shown that for macro-scale chirality, the grain-pair interactions must include coupling between normal and tangential deformations. We have designed such a grain-pair connection for physical realization and quantified with FE model. The verification of the prediction is then performed using a physical model of 1D bead string obtained by 3D printing. The behavior is also verified using a discrete model of 1D bead string.

Keywords: granular micromechanics; chiral metamaterial; micromorphic continuum; micro-macro identification; discrete element.

1. Introduction

Metamaterials may be considered as materials that are conceived to achieve predetermined behavior. Predictive theories are key for metamaterial design based upon needs and possibilities; as are the technologies for the synthesis of the designed material. Recent developments in additive manufacturing has opened possibilities of realizing a variety of microstructures that were otherwise difficult to fabricate (De Angelo et al., 2019b; dell'Isola et al., 2019; Misra et al., 2018a; Nejadsadeghi et al., 2019a). Furthermore, recent work on revealing the connections of higher gradient continuum terms to the micro-mechanisms within a materials have led to development of interesting predictive theories. In this regard, the pioneering work on 2nd and higher gradient theories leading to pantographic metamaterials is particularly worthy to highlight (Abdoul-Anziz and Seppecher, 2018; Alibert et al., 2003; dell'Isola et al., 2016; dell'Isola et al., 2018; Seppecher et al., 2011). On the other hand, granular materials have been shown to require the introduction of additional degrees-of-freedom predicated by their micro-mechanisms that are contributed by the inter-play of grain-pair interactions and granular arrangement – collectively termed as mechano-morphology, leading to higher-order theories or micromorphic continuum theories (Nejadsadeghi and Misra, 2019b). Indeed, in a series of papers, we have shown through theoretical considerations that for granular materials, the classical continuum model is not sufficient, and instead non-standard enhanced continuum model based upon the granular micromechanics approach (GMA) is generally required for representing the grain-scale deformation modes with increasing accuracy (see for example the higher-order or micromorphic theories (Misra and Poorsolhjouy, 2016b; Misra and Poorsolhjouy, 2017; Nejadsadeghi and Misra, 2019b; Poorsolhjouy and Misra, 2019). The GMA provides a paradigm that bridges the discrete models to appropriate continuum model. In this paper, we utilize the predictions of GMA to design and synthesize through additive manufacturing granular (meta) material with specific properties. In particular, we have shown through closed-form derived expressions for elastic constants that grain interactions that include coupling between normal and tangential deformations result in macro-scale chiral behavior for 2D isotropic granular media. We have then designed such a coupled grain-interaction for incorporation into physical models. We have evaluated the behavior of 1D granular material with the designed grain interaction through independent experiments and numerical simulations. First, finite element (FE) model was utilized to quantify the grain-pair interaction by modeling the grains and their connection as classical Cauchy continua. Then 3D printing was used to realize the 1D granular model in which the grain-pair connections are those evaluated with the FE model. Finally, to verify the GMA prediction, we use the discrete model in which grains are modeled as rigid beads connected via springs whose constants are specified based upon the FE model of a grain-pair interaction.

2. Review of GMA based Micromorphic Continuum Model of Degree 1

The GMA (Misra et al., 2019; Misra and Poorsolhjouy, 2017) follows a pathway that shares affinity with Piola's concepts of continuum description of materials as a necessary approximation of a molecular view (dell'Isola et al., 2014; dell'Isola et al., 2015; Eugster and dell'Isola, 2017). At the spatial scale in which we seek the continuum description, the individual grains and their motions are latent (concealed). However, it is these grain motions that determine the deformation of a representative volume element (RVE) containing numerous grains, and consequently, the mapping of a continuum material point from undeformed to deformed configuration in a macro-body composed of such material. In GMA, the continuum description is achieved by (i) expressing grain-scale motions in terms of continuum kinematic measures, (ii) identifying the volume average of grain-pair interaction energies with the macro-scale deformation energy density, and finally (iii) applying variational approach for defining stress/force conjugates of the kinematic variables, determining constitutive relations, and the governing Euler-Lagrange equations (Misra and Poorsolhjouy, 2016b; Misra and Poorsolhjouy, 2017; Nejadsadeghi and Misra, 2019b; Poorsolhjouy and Misra, 2019).

Let us consider a granular material system that is homogeneous at the continuum scale. To describe the grain motions and the relevant continuum kinematic measures for such a granular system, two coordinate systems are considered as shown in Figure 1. One at the micro-scale, denoted by $\boldsymbol{x'}$, attached to the continuum material point (RVE) with its origin set to the barycenter of the RVE in which the grains and their motions are visible. The other at the macro-scale, denoted by $\boldsymbol{x}$, with its coordinate axes parallel to those of $\boldsymbol{x'}$, in which the homogeneous macro-body is placed. The displacement field of grain centroids, ϕ_i, is conveniently written as (Nejadsadeghi and Misra, 2019b)

$$\phi_i = \bar{\phi}_i(x_m) + \psi^{\phi}_{ij}(x_m)x'_j + \psi^{\phi}_{ijk}(x_m)x'_j x'_k, \quad (1)$$

where $\bar{\phi}_i$ is the macro-scale displacement field, and quantities ψ^{ϕ}_{ij} and ψ^{ϕ}_{ijk}, functions of macro-scale coordinates $\boldsymbol{x}$, are termed as the second and the third rank micro-deformation tensors. In this work, as a constitutive choice, we choose to terminate the expression at the 2nd order, although additional higher-order terms can be considered as discussed in (Nejadsadeghi and Misra, 2019b). Clearly, the assumption in Eq. 1 provides a method to capture the relative motions of grains with respect to macro-scale displacement field, such as the experimentally reported displacement fluctuations in granular packing subjected to homogeneous boundary displacements compatible with a linear displacement field (Misra, 1998; Misra and Jiang, 1997; Richefeu et al., 2012). Indeed, non-affinity of grain motion are well-known (see for example (Misra and Chang, 1993)). The non-affinity arises due to a variety of factors, including irregularity of granular structure, spatial variability and high contrast of grain interactions (stiff or soft), and the peculiar and non-local nature of grain interactions. In this case, the micro-deformation tensors play the role of enriching the kinematical description of grain motions within the RVE. Throughout the paper, the summation convention over repeated indices is implied unless explicitly noted otherwise.

We proceed by considering the relative displacement of two (contacting) neighboring grains, *n* and *p*. Using Eq. 1, the displacement of the grain *p* centroid is expressed in terms of the displacement of the neighbor grain, *n*, centroid as follows

$$\delta^{np}_i = \phi^p_i - \phi^n_i = \psi^{\phi}_{ij} l^{np}_j + \psi^{\phi}_{ijk} J^{np}_{jk} \quad (2)$$

where $l^{np}_j = x'^p_j - x'^n_j$ is a grain-pair branch vector joining the centroids of grains *n* and *p*, the tensor product $J^{np}_{jk} \approx l^{np}_j l^{np}_k / 2$ is the gyration tensor. To clarify the meaning of the micro-deformation tensors, we now introduce the following relative deformation tensors

$$\gamma^{\phi}_{ij} = \bar{\phi}_{i,j} - \psi^{\phi}_{ij} \text{ and } \gamma^{\phi}_{ijk} = \psi^{\phi}_{ij,k} - \psi^{\phi}_{ijk} \quad (3)$$

where comma in the subscript denotes differentiation with respect to the spatial coordinates. In Eq. 3, the differentiation is with respect to the macro-scale coordinates $\boldsymbol{x}$, and defines the macro-scale gradients of the macro displacement field $\bar{\phi}_i$, and micro-deformation tensor ψ^{ϕ}_{ij}. We further assume that the 3rd rank relative deformation tensor γ^{ϕ}_{ijk} vanishes, such that $\psi^{\phi}_{ijk} = \psi^{\phi}_{ij,k}$. In this case, the micro-deformation tensor ψ^{ϕ}_{ijk} is no longer independent, but depends upon the micro-deformation tensor ψ^{ϕ}_{ij} . The assumption is similar to that introduced in Euler beam model, wherein the rotational degree of freedom is related to the gradient of vertical deflection. Furthermore, considering the smallness of the RVE in the continuum view, we exploit Taylor's expansion to identify the micro-deformation tensors in Eq. 2 as the gradients of ϕ_i with respect to micro-scale coordinates, ***x'***, such that

$$\psi^{\phi}_{ij} \triangleq \quad \text{and} \quad \psi^{\phi}_{ijk} \triangleq \qquad (4)$$

where $\phi_{i,j}$ and $\phi_{i,jk}$ are termed as micro-gradients.

In view of Eq. 3 and the identification in Eq. 4, we can say that the micro-gradient field, $\phi_{i,j}$, is decomposed into a part identical to the macro-gradient, $\bar{\phi}_{i,j}$ (where gradient is with respect to ***x***) whose symmetric components form the classical infinitesimal strain tensor, and a second part called relative micro-gradient, γ^{ϕ}_{ij}, representing the micro-scale fluctuations from the macro-gradient. The described decomposition bears similarity to that introduced in micro-structural elasticity of (Mindlin, 1964) as well as in micromorphic mechanics (Eringen, 1999; Germain, 1973). It is evident that for this micromorphic model, the relative micro-gradient, γ^{ϕ}_{ij}, is independent of ***x'*** (constant within the RVE). Furthermore, the micro-gradient field, $\phi_{i,jk}$, which represents the 2nd gradient (with respect to ***x'***) of the grain displacement field, is given as the macro-gradient (with respect to ***x***) of the micro-deformation tensor field $\psi^{\phi}_{ij,k}$. These assumptions, which lead to a micromorphic model of degree 1 according to (Germain, 1973), implies that the grain displacement field within the RVE must be estimated by a function twice differentiable in ***x'*** (such as a polynomial of degree 2). For further discussions of GMA based higher-order models, the reader is directed to (Nejadsadeghi and Misra, 2019b) which describes the kinematics of micromorphic model of degree *n* as well as its devolution to micromorphic models of degrees 2 and 1, and to micro-polar modes and 2nd gradient models.

Combining Eqs. 2 and 3 along with the assumption $\psi^{\phi}_{ijk} = \psi^{\phi}_{ij,k}$, the relative displacement of two neighbor grains, *n* and *p*, is found as

$$\delta^{np}_i = \phi^p_i - \phi^n_i = \left(\bar{\phi}_{i.j} - \gamma^{\phi}_{ij}\right) l^{np}_j + \psi^{\phi}_{ij,k} J^{np}_{jk} = \delta^M_i - \delta^m_i + \delta^g_i \qquad (5)$$

Where the components related to the macro-gradient, $\bar{\phi}_{i,j}$, the relative micro-gradient, γ^{ϕ}_{ij}, and the macro-gradients of the micro-deformation tensor field $\psi^{\phi}_{ij,k}$, are, respectively

$$\delta^M_i = \bar{\phi}_{i,j} l^{np}_j; \quad \delta^m_i = \gamma^{\phi}_{ij} l^{np}_j; \quad \delta^g_i = \psi^{\phi}_{ij,k} J^{np}_{jk} \qquad (6)$$

Further, the relative rotation of grains within the granular assembly can be related to the rotation field within the material point defined as the curl of displacement field (Misra and Poorsolhjouy, 2016b). Now using this definition of rotation and applying Taylor series expansion, the relative rotation of two neighbor grains, n and p, denoted as $\boldsymbol{\theta}$ is obtained as (using Eq. 3)

$$\theta^u_i = \kappa^p_i - \kappa^n_i = \kappa^n_{i,p} l^{np}_j = \left(e_{ijk}\phi_{k,j}\right)_{,p} l^{np}_j = e_{ijk}\psi^{\phi}_{kj,p} l^{np}_j \qquad (7)$$

where κ^p_i is the vector of rotation of p[th] grain. The grain-pair relative rotation between two interacting grains is, thus, related to the second gradient term, $\phi_{i,jk}$, or equivalently the macro-gradients of the micro-defromation tensor field $\psi^{\phi}_{ij,k}$. Thus, Eqs. 6 and 7 provide an identification of the macro-micro kinematic variables. It is noted here that the relative rotation in Eq. 7 does not consider grain spins which could be significant in some granular systems (Poorsolhjouy and Misra, 2019) and are known from measurements of kinematic fields in grain assembles (Misra, 1998; Misra and Jiang, 1997) as well as simulation using discrete granular models (Misra et al., 2018b; Turco et al., 2019).

Using the micro-macro identification in Eqs. 5 through 7, the deformation energy density, *W*, of a granular RVE can be expressed in terms of both the macro-scale kinematic measures, and the micro-scale kinematic measures as follows:

$$W = W\left(\bar{\phi}_{(i,j)}, \gamma^{\phi}_{ij}, \psi^{\phi}_{ij,k}\right) = \frac{1}{V}\sum_{\alpha} W^{\alpha}\left(\delta^{\alpha M}_i, \delta^{\alpha m}_i, \delta^{\alpha g}_i, \theta^{\alpha u}_i\right) \qquad (8)$$

where W^{α} is the grain-pair deformation energy and the summation runs over all grain-pair contacts, α. Strain rate tensors as those introduced in (Altenbach and Eremeyev, 2014) could be used to extend the analysis to finite deformations. Macro-scale objective energy, particularly for the large deformation problems of granular materials, is discussed with respect to material symmetry group for micromorphic media in (Eremeyev, 2018). The micro-macro identification of kinematical quantities in Eqs. 5 and 6 along with those of the deformation energies given in Eq. 8, leads to a micromorphic continuum model of degree 1 whose governing equations and constitutive relationships are given in (Misra and Poorsolhjouy, 2016b). In this regard, a set of micro-scale constitutive equations that link the micro-scale kinematics measures to their conjugate force and moment measures have been introduced where following the D'Alembertian viewpoint, as also those of Lagrange, Piola and Hellinger among others (see for example (Oliveira, 2017) and (Eugster and dell'Isola, 2017, 2018a, b)), the grain-pair forces and moments are defined as,

$$f_i^{\alpha\xi} = \frac{\partial W^\alpha}{\partial \delta_i^{\alpha\xi}}, \quad \text{where } \xi\text{: M, m, } g; \quad \text{and } m_i^{\alpha u} = \frac{\partial W^\alpha}{\partial \theta_i^{\alpha u}} \tag{9}$$

such that

$$\begin{aligned} f_i^{\alpha\xi} &= K_{ij}^{\alpha\xi}\delta_j^{\alpha\xi} + D_{ij}^{\alpha\xi}\theta_j^{\alpha u}; \qquad \text{where } \xi\text{: M, m, g} \\ m_i^{\alpha u} &= D_{ij}^{\alpha\xi}\delta_j^{\alpha\xi} + G_{ij}^{\alpha u}\theta_j^{\alpha u}; \end{aligned} \tag{10}$$

Further the macro-scale stress measures can be defined as conjugates to each of the continuum kinematic variables, such that the following macro-scale constitutive equations are obtained (see for example (Misra and Poorsolhjouy, 2016a))

$$\tau_{ij} = \frac{\partial W}{\partial \bar{\phi}_{(i,j)}} = \frac{1}{V}\sum_\alpha f_i^{\alpha M} l_j^\alpha = \frac{1}{V}\sum_\alpha K_{ik}^{\alpha M}\delta_k^\alpha l_j^\alpha = \left(\frac{1}{V}\sum_\alpha K_{ik}^{\alpha M} l_l^\alpha l_j^\alpha\right)\bar{\phi}_{(i,j)} = C_{ijkl}^M \bar{\phi}_{(i,j)} \tag{11a}$$

$$\begin{aligned} \sigma_{ij} &= \frac{\partial W}{\partial \gamma_{ij}^\phi} = \frac{1}{V}\sum_\alpha f_i^{\alpha m} l_j^\alpha = \frac{1}{V}\sum_\alpha \left(K_{ik}^{\alpha m}\delta_k^{\alpha m} l_j^\alpha + D_{ik}^{\alpha m}\theta_k^{\alpha u} l_j^\alpha\right) \\ &= \left(\frac{1}{V}\sum_\alpha K_{ik}^{\alpha m} l_l^\alpha l_j^\alpha\right)\gamma_{kl}^\phi + \left(\frac{1}{V}\sum_\alpha D_{ip}^{\alpha m} e_{plk} l_m^\alpha l_j^\alpha\right)\psi_{kl,m}^\phi = C_{ijkl}^m \gamma_{kl}^\phi + D_{ijklm}^m \psi_{kl,m}^\phi \end{aligned} \tag{11b}$$

$$\begin{aligned} \mu_{ijk} &= \frac{\partial W}{\partial \psi_{ij,k}^\phi} = \frac{1}{V}\sum_\alpha \left(f_i^{\alpha g} J_{jk}^\alpha + m_l^{\alpha u} e_{jil} l_k^\alpha\right) \\ &= \left(\frac{1}{V}\sum_\alpha D_{pl}^{\alpha m} e_{jip} l_k^\alpha l_m^\alpha\right)\gamma_{lm}^\phi + \left(\frac{1}{V}\sum_\alpha K_{il}^g J_{mn}^\alpha J_{jk}^\alpha + \frac{1}{V}\sum_\alpha G_{pq}^u e_{mlq} e_{jip} l_k^\alpha l_n^\alpha\right)\psi_{ij,k}^\phi \\ &= \tilde{I} \qquad A_{ijklmn}^g + A_{ijklmn}^u\big)\psi_{lm,n}^\phi = D_{ijklm}^m \gamma_{lm}^\phi + A_{ijklmn}\psi_{lm,n}^\phi \end{aligned} \tag{11c}$$

In Eq. 11, τ_{ij}, is the Cauchy stress with symmetry imposed (not explicitly expressed in Eq. 11a), and σ_{ij} is the asymmetric relative stress, and μ_{ijk} is the double stress tensor. The fourth rank constitutive tensors C_{ijkl}^{M} and C_{ijkl}^{m} represent stiffness relating to macro-strain and relative micro-gradient, respectively, the fifth rank tensor D_{ijklm}^{m} couples relative micro-gradient and macro-gradients of the micro-deformation, and the sixth rank tensor A_{ijklmn} represent stiffness corresponding to the second gradient of micro-displacements.

3. Predicted 2D Isotropic Chiral Granular Material

As is standard in GMA, the grain-pair interactions can be defined in a local Cartesian coordinate system formed of the unit vector along the axis joining the centroids of the two grains, termed as the normal direction, and unit vector along two arbitrarily chosen orthogonal axes lying on the plane orthogonal to the normal direction, termed as the tangential plane. For the case of 2D granular systems, in which the interactions is between disk-like objects, the grain-pair interactions are defined in the local coordinate system composed of a unit normal vector, n_i, and the tangential unit vector, s_i, given as

$$\begin{aligned} n_i &= \langle \cos\theta, \sin\theta \rangle \\ s_i &= \langle -\sin\theta, \cos\theta \rangle \end{aligned} \tag{12}$$

where θ is the polar angle of the 2D polar coordinate system.

3.1 Grain-pair elasticity

We now consider the following grain-pair elastic deformation energy in terms of the grain-scale kinematic quantities defined in Eqs. 5 and 6, given as

$$W^{\alpha} = \frac{1}{2}\left[\begin{array}{l} K_n^{\alpha M}\left(\delta_n^{\alpha M}\right)^2 + K_s^{\alpha M}\left(\delta_s^{\alpha M}\right)^2 + K_n^{\alpha m}\left(\delta_n^{\alpha m}\right)^2 + K_s^{\alpha m}\left(\delta_s^{\alpha m}\right)^2 + 2K_{ns}^{\alpha m}\left(\delta_n^{\alpha m}\delta_s^{\alpha m}\right) + \\ K_n^{\alpha g}\left(\delta_n^{\alpha g}\right)^2 + K_s^{\alpha g}\left(\delta_s^{\alpha g}\right)^2 + 2D_n^{\alpha u}\left(\delta_n^{\alpha m}\theta_3^{\alpha u}\right) + 2D_s^{\alpha u}\left(\delta_s^{\alpha m}\theta_3^{\alpha u}\right) + G_3^{\alpha u}\left(\theta_3^{\alpha u}\right)^2 \end{array}\right] \tag{13}$$

Where the subscripts are used to denote the quantities along the local coordinate axes (these subscripts do not follow tensor summation convention). In Eq. 13 the coupling terms have been retained only for the grain-pair relative displacement components related to the relative micro-gradient, and those with the grain-pair relative rotations. This choice of deformation energy will lead to a desired particular form of continuum model. Using the assumed energy expression in Eq. 13, the grain-pair (micro-scale) constitutive relations can be written as follows

$$\begin{Bmatrix} f_n^{\alpha M} \\ f_s^{\alpha M} \end{Bmatrix} = \begin{bmatrix} K_n^{\alpha M} & 0 \\ 0 & K_s^{\alpha M} \end{bmatrix} \begin{Bmatrix} \delta_n^{\alpha M} \\ \delta_s^{\alpha M} \end{Bmatrix} \tag{14a}$$

$$\begin{Bmatrix} f_n^{\alpha m} \\ f_s^{\alpha m} \end{Bmatrix} = \begin{bmatrix} K_n^{\alpha m} & K_{ns}^{\alpha m} \\ K_{ns}^{\alpha m} & K_s^{\alpha m} \end{bmatrix} \begin{Bmatrix} \delta_n^{\alpha m} \\ \delta_s^{\alpha m} \end{Bmatrix} + \begin{bmatrix} D_n^{\alpha u} \\ D_s^{\alpha u} \end{bmatrix} \left\{ \theta_3^{\alpha u} \right\} \tag{14b}$$

$$\begin{Bmatrix} f_n^{\alpha g} \\ f_s^{\alpha g} \end{Bmatrix} = \begin{bmatrix} K_n^{\alpha g} & 0 \\ 0 & K_s^{\alpha g} \end{bmatrix} \begin{Bmatrix} \delta_n^{\alpha g} \\ \delta_s^{\alpha g} \end{Bmatrix} \tag{14c}$$

$$\left\{ m_3^{\alpha u} \right\} = \begin{bmatrix} D_n^{\alpha u} & D_s^{\alpha u} \end{bmatrix} \begin{Bmatrix} \delta_n^{\alpha m} \\ \delta_s^{\alpha m} \end{Bmatrix} + \begin{bmatrix} G_3^{\alpha u} \end{bmatrix} \left\{ \theta_3^{\alpha u} \right\} \tag{14d}$$

For further derivation, the above constitutive relations can be rotated to the RVE coordinate system to result in the following stiffness tensor (as in Eq. 10)

$$K_{ij}^{\alpha M} = \begin{bmatrix} K_{11}^{\alpha M} & K_{12}^{\alpha M} \\ K_{12}^{\alpha M} & K_{22}^{\alpha M} \end{bmatrix} = \begin{bmatrix} n_1^\alpha & s_1^\alpha \\ n_2^\alpha & s_2^\alpha \end{bmatrix} \begin{bmatrix} K_n^{\alpha M} & 0 \\ 0 & K_s^{\alpha M} \end{bmatrix} \begin{bmatrix} n_1^\alpha & n_2^\alpha \\ s_1^\alpha & s_2^\alpha \end{bmatrix} \tag{15a}$$

$$K_{ij}^{\alpha m} = \begin{bmatrix} K_{11}^{\alpha m} & K_{12}^{\alpha m} \\ K_{12}^{\alpha m} & K_{22}^{\alpha m} \end{bmatrix} = \begin{bmatrix} n_1^\alpha & s_1^\alpha \\ n_2^\alpha & s_2^\alpha \end{bmatrix} \begin{bmatrix} K_n^{\alpha m} & K_{ns}^{\alpha m} \\ K_{ns}^{\alpha m} & K_s^{\alpha m} \end{bmatrix} \begin{bmatrix} n_1^\alpha & n_2^\alpha \\ s_1^\alpha & s_2^\alpha \end{bmatrix} \tag{15b}$$

We note that the stiffness tensor $K_{ij}^{\alpha g}$ has the same structure as Eq. 15a, and for the 2D case the stiffness tensors $D_{ij}^{\alpha u}$ and $G_{ij}^{\alpha u}$ will reduce as follows since the only relevant rotation is $\theta_3^{\alpha u}$

$$D_{i3}^{\alpha u} = \begin{bmatrix} D_1^{\alpha u} \\ D_2^{\alpha u} \end{bmatrix} = \begin{bmatrix} n_1^\alpha & s_1^\alpha \\ n_2^\alpha & s_2^\alpha \end{bmatrix} \begin{bmatrix} D_n^{\alpha u} \\ D_s^{\alpha u} \end{bmatrix} \text{ and } \mathrm{G}_{33}^{\alpha u} = \begin{bmatrix} G_3^{\alpha u} \end{bmatrix} \tag{15c}$$

3.2 Directional averaging of constitutive behavior

We further note that the quantities within the summations in Eq. 11 are functions of the orientations of the branch vector and the product of grain-pair stiffness and branch length. In this case, the average value of product of branch vector length and stiffness coefficients and its directional distribution can be used as the micromechanical model parameter (see for a discussion (Misra and Poorsolhjouy, 2016c)). For the 2D format of the GMA, an identification process of the constitutive relationships were presented in (Misra and Poorsolhjouy, 2015, 2016a). As an example, the summation in Eq. 11a over all grain-pairs can be rewritten using Eq. 15a as

$$C_{ijkl}^{M}=\frac{1}{V}\sum_{\alpha}K_{ik}^{\alpha M}l_l^{\alpha}l_j^{\alpha}=\frac{1}{V}\sum_{\alpha=1}^{N}n_l^{\alpha}n_j^{\alpha}\left(\left(l^{\alpha}\right)^2K_n^{\alpha M}n_i^{\alpha}n_k^{\alpha}+\left(l^{\alpha}\right)^2K_s^{\alpha M}s_i^{\alpha}s_k^{\alpha}\right)\qquad i,j,k,l=1,2 \tag{16}$$

which can be further sorted and binned according to grain-pair orientations and recast as summation over the polar angle θ as

$$C_{ijkl}^{M}=\frac{1}{V}\sum_{\theta}\left(\sum_{\rho}^{N^{\rho}}\left(l^{\rho}\right)^2K_n^{\rho M}\right)n_l^{\alpha}n_j^{\alpha}n_i^{\alpha}n_k^{\alpha}+\left(\sum_{\rho}^{N^{\rho}}\left(l^{\rho}\right)^2K_s^{\rho M}\right)n_l^{\alpha}n_j^{\alpha}s_i^{\alpha}s_k^{\alpha}\qquad i,j,k,l=1,2 \tag{17}$$

where $N^{\rho}\left(\theta\right)$ is the total number of grain-pair for a given polar angle bin θ, such that

$$N=\sum_{\theta}N^{\rho}\left(\theta\right) \tag{18}$$

where N is the count of grain-pairs in the RVE and the summation over ρ is the sum of the product of branch length square and the grain-pair stiffness (for example $\left(l^{\rho}\right)^2K_n^{\rho M}$) for all grain-pairs in that bin. For granular material systems with many different grain-sizes, grain shapes and types of grain-pair interactions (which as combination can be termed as micro-scale mechano-morphology), these sums will be different for different polar angles. This variation with polar angles can be treated by defining directional distribution functions. Since branch length and stiffnesses appear as products, their directional distribution density cannot be defined independently, therefore, we introduce the directional density distribution function, $\xi(\theta)$, defined as

$$\xi\left(\theta\right)=\frac{\sum_{\rho}\left(l^{\rho}\right)^2K_n^{\rho M}}{\sum_{\alpha=1}^{N}\left(l^{\alpha}\right)^2K_n^{\alpha M}}=\frac{\sum_{\rho}\left(l^{\rho}\right)^2K_s^{\rho M}}{\sum_{\alpha=1}^{N}\left(l^{\alpha}\right)^2K_s^{\alpha M}} \tag{19}$$

where, for simplicity, we have assumed that grain-pair behavior in the normal and shear directions follow the same distribution. It is evident that the directional density distribution function, $\xi(\theta)$, represents the relative measure of material stiffness in a given direction resulting from a combination of grain-size, the number of grain-pair interactions and the grain-pair stiffness. Further, it is useful to define an average product of branch length square and the grain-pair stiffness, l^2K_n ,as

$$l^2 K_n^M = \frac{\sum_{\alpha=1}^{N} \left(l^\alpha\right)^2 K_n^\alpha}{N}; \qquad l^2 K_s^M = \frac{\sum_{\alpha=1}^{N} \left(l^\alpha\right)^2 K_n^\alpha}{N} \tag{20}$$

where l may be regarded as the average branch length, K_n^M and K_s^M as the average grain-pair stiffnesses for the material, and $\rho^c = V / N$ is the number density of grain-pair interactions. Thus, using Eqs. 19 and 20, the following integral form of Eq. 17 can be obtained

$$C_{ijkl}^M = l^2 \rho^c \int_{\theta=0}^{2\pi} \left(K_{ik}^M n_j n_l\right) \xi d\theta \tag{21a}$$

Similar considerations for Eqs. 11b-11d will yield the following

$$C_{ijkl}^m = l^2 \rho^c \int_{\theta=0}^{2\pi} \left(K_{ik}^m n_j n_l\right) \xi d\theta \tag{21b}$$

$$D_{ijklm}^m = l^2 \rho^c \int_{\theta=0}^{2\pi} \left(D_{i3}^m e_{3lk} n_m n_j\right) \xi d\theta \tag{21c}$$

$$A_{ijklmn} = l^2 \rho^c \int_{\theta=0}^{2\pi} \frac{l^2}{4} \left(K_{il}^g n_j n_k n_m n_n\right) + \left(G_{33}^u e_{lm3} e_{ij3} n_k n_n\right) \xi d\theta \tag{21d}$$

where we have assumed that all types of grain-pair mechanisms follow the same directional distributions. For isotropic materials (or for randomly grain assemblies of various grain sizes, grain shapes and grain-pair interactions) the density distribution function in 2D domains is simply

$$\xi\left(\theta\right) = \frac{1}{2\pi} \Rightarrow \int_{\theta} \xi d\theta = \frac{1}{2\pi} 2\pi = 1; \tag{22}$$

3.3 Expressions for the constitutive coefficients and nature of chirality

As a result, the predicted 2D form of constitutive relationship and corresponding stiffness tensor for the macro-strain, $\bar{\phi}_{(i,j)} = \varepsilon_{ij}$, is obtained in an explicit form by integrating Eq. 21a. The resultant 3×3 stiffness matrix can be written using the Vogt notation by explicitly considering the symmetry of the strain tensor, and thus that of the conjugate Cauchy stress tensor as follows:

$$\begin{Bmatrix} \tau_{11} \\ \tau_{22} \\ \tau_{12} \end{Bmatrix} = \begin{pmatrix} C_{11}^M & C_{12}^M & 0 \\ C_{12}^M & C_{11}^M & 0 \\ 0 & 0 & C_{33}^M \end{pmatrix} \begin{Bmatrix} \varepsilon_{11} \\ \varepsilon_{22} \\ 2\varepsilon_{12} \end{Bmatrix}; \tag{23a}$$

where

$$C_{11}^{M}=\frac{l^{2}\rho^{c}}{8}\left(3K_{n}^{M}+K_{s}^{M}\right);\quad C_{12}^{M}=\frac{l^{2}\rho^{c}}{8}\left(K_{n}^{M}-K_{s}^{M}\right);\text{ and} \tag{23b}$$

$$C_{33}^{M}=\frac{l^{2}\rho^{c}}{8}\left(K_{n}^{M}+K_{s}^{M}\right)=\frac{C_{11}^{M}-C_{12}^{M}}{2}$$

The obtained stiffness matrix in Eq. 23 is invariant to rotation and reflection transformations generated by the rotation matrix $R(\theta)=\begin{pmatrix}\cos\theta & -\sin\theta\\ \sin\theta & \cos\theta\end{pmatrix}$ and reflection, say about the y-axis $M_{y}=\begin{pmatrix}-1 & 0\\ 0 & 1\end{pmatrix}$. Based upon the macro-scale stiffnesses, the material belongs to symmetry class [O(2)], and the stiffness matrix is characterized by only 2 independent constants as expected for 2D isotropic materials (Auffray et al., 2015; He and Zheng, 1996).

The predicted 2D form of constitutive relationship and corresponding stiffness tensor for the relative stress and micro-gradient, $\gamma_{ij}^{\phi}=\bar{\phi}_{i.j}-\psi_{ij}^{\phi}$, is obtained from Eq. 21b as follows

$$\begin{Bmatrix}\sigma_{11}\\ \sigma_{22}\\ \sigma_{12}\\ \sigma_{21}\end{Bmatrix}=\begin{bmatrix}C_{1111}^{m} & C_{1122}^{m} & C_{1112}^{m} & C_{1121}^{m}\\ C_{1122}^{m} & C_{1111}^{m} & C_{1112}^{m} & C_{1121}^{m}\\ C_{1112}^{m} & C_{1112}^{m} & C_{1212}^{m} & C_{1122}^{m}\\ C_{1121}^{m} & C_{1121}^{m} & C_{1122}^{m} & C_{1212}^{m}\end{bmatrix}\begin{Bmatrix}\gamma_{11}\\ \gamma_{22}\\ \gamma_{12}\\ \gamma_{21}\end{Bmatrix}+\left(D_{ijklm}^{m}\right)_{4x8}\begin{Bmatrix}\psi_{11,1}\\ \psi_{11,2}\\ \psi_{12,1}\\ \psi_{12,2}\\ \psi_{21,1}\\ \psi_{21,2}\\ \psi_{22,1}\\ \psi_{22,2}\end{Bmatrix} \tag{24}$$

where

$$C_{1111}^{m}=\frac{l^{2}\rho^{c}}{8}\left(3K_{n}^{m}+K_{s}^{m}\right);\; C_{1122}^{m}=\frac{l^{2}\rho^{c}}{8}\left(K_{n}^{m}-K_{s}^{m}\right); \tag{25}$$

$$C_{1212}^{m}=\frac{l^{2}\rho^{c}}{8}\left(K_{n}^{m}+3K_{s}^{m}\right)=C_{1111}^{m}-2C_{1122}^{m};\quad C_{1112}^{m}=-C_{1121}^{m}=\frac{-l^{2}\rho^{c}}{4}K_{ns}^{m};$$

The stiffness matrix in Eq. 24 has 3 independent constants and is invariant to rotation transformation, and is therefore, classified as isotropic. The stiffness matrix, however, does not satisfy the mirror invariance. On the basis of this micro-scale stiffness matrix, the material could be said to belong to symmetry class [SO(2)]. In this type of isotropic material, *chirality* is present due to the anti-symmetric coupling between the normal and the shear terms given by $C^m_{1112} = -C^m_{1121}$, which are concerned with the first-order phenomena.

Interestingly, the 5-th rank tensor, D^m_{ijklm}, is identically zero. It is remarked, however, that the 5-th rank tensor is, in general, non-zero for non-centro symmetric 2D structure and could be non-zero for 2D structures that yield isotropic classical (Cauchy) elasticity for either chiral or achiral structures. The symmetry classes for the 5-th rank stiffness tensor as well as for 2nd gradient elasticity has been discussed in (Auffray et al., 2015). An experimental evaluation of particular microstructure that leads to a material of symmetry class $\left[Z_2^\pi\right]$ with non-zero 5-th rank tensor as well as possible chirality has been shown in (Poncelet et al., 2018)). Finally, the predicted 2D form of constitutive relationship and corresponding stiffness tensor for the (macro-) gradient of the micro-gradient tensor, $\psi^\phi_{ij,k}$, can be obtained from Eq. 21d as give in (Misra and Poorsolhjouy, 2016a). Chiral behavior for materials of symmetry class [SO(2)] can originate from certain coupling within this higher-order stiffness matrix as discussed in (Auffray et al., 2015). Indeed, the stiffness matrix reported in (Misra and Poorsolhjouy, 2016a) shows the possibility of these coupling, however, the mechanisms that give rise to the relevant non-zero terms need further considerations and will be discussed in a future paper. The 6-th rank stiffness tensor will not be discussed further in this paper, and for this reason, its expression is not repeated here.

3.4 Micro-scale mechanism of chirality and relation to classical micropolar continuum

It is noteworthy that the two stiffness tensors, C^M_{ijkl} and C^m_{ijkl}, bear formal similarity. The differences arise from the nature of grain-pair deformation mechanism the two represent (as noted by the different grain-pair stiffness coefficients). Since the relative micro-gradient is, in general asymmetric, it is instructive to rewrite Eq. 24 in terms of the symmetric, $\gamma^\phi_{(ij)}$, and antisymmetric, $\gamma^\phi_{[ij]}$, parts of the micro-gradient tensor as:

$$\sigma_{(ij)} = C^m_{(ij)(kl)}\gamma^\phi_{(ij)} + C^m_{(ij)[kl]}\gamma^\phi_{[ij]} \tag{26a}$$

$$\sigma_{[ij]} = C^m_{[ij](kl)}\gamma^\phi_{(ij)} + C^m_{[ij][kl]}\gamma^\phi_{[ij]} \tag{26b}$$

Or alternatively

$$\sigma_{(ij)} = C^m_{(ij)(kl)}\left(\bar{\phi}_{(k.l)} - \psi^{\phi}_{(kl)}\right) + C^m_{(ij)[kl]}\left(\bar{\phi}_{[k.l]} - \psi^{\phi}_{[kl]}\right) \tag{27a}$$

$$\sigma_{[ij]} = C^m_{[ij](kl)}\left(\bar{\phi}_{(k,l)} - \psi^{\phi}_{(kl)}\right) + C^m_{[ij][kl]}\left(\bar{\phi}_{[k,l]} - \psi^{\phi}_{[kl]}\right) \tag{27b}$$

where:

$$C^m_{(ij)(kl)} = \frac{C^m_{ijkl} + C^m_{jikl} + C^m_{ijlk} + C^m_{jikl}}{4}; \qquad C^m_{(ij)[kl]} = \frac{C^m_{ijkl} + C^m_{jikl} - C^m_{ijlk} - C^m_{jikl}}{4} \tag{28a}$$

$$C^m_{[ij](kl)} = \frac{C^m_{ijkl} - C^m_{jikl} + C^m_{ijlk} - C^m_{jikl}}{4}; \qquad C^m_{[ij][kl]} = \frac{C^m_{ijkl} - C^m_{jikl} - C^m_{ijlk} + C^m_{jikl}}{4} \tag{28b}$$

Which, using matrix notation, can be written as

$$\begin{Bmatrix} \sigma_{11} \\ \sigma_{22} \\ \dfrac{\sigma_{12}+\sigma_{21}}{2} \end{Bmatrix} = \begin{pmatrix} C^m_{11} & C^m_{12} & 0 \\ C^m_{12} & C^m_{11} & 0 \\ 0 & 0 & \dfrac{C^m_{11}-C^m_{12}}{2} \end{pmatrix} \begin{Bmatrix} \gamma_{11} \\ \gamma_{22} \\ \gamma_{12}+\gamma_{21} \end{Bmatrix} + \begin{pmatrix} 0 & 0 & C^m_{13} & -C^m_{13} \\ 0 & 0 & C^m_{13} & -C^m_{13} \\ 0 & 0 & 0 & 0 \end{pmatrix} \begin{Bmatrix} \gamma_{11} \\ \gamma_{22} \\ \gamma_{12}-\gamma_{21} \\ \gamma_{21}-\gamma_{12} \end{Bmatrix} \tag{29a}$$

$$\begin{Bmatrix} \sigma_{11} \\ \sigma_{22} \\ \dfrac{\sigma_{12}-\sigma_{21}}{2} \\ \dfrac{\sigma_{21}-\sigma_{12}}{2} \end{Bmatrix} = \begin{pmatrix} 0 & 0 & 0 \\ 0 & 0 & 0 \\ C^m_{13} & C^m_{13} & 0 \\ -C^m_{13} & -C^m_{13} & 0 \end{pmatrix} \begin{Bmatrix} \gamma_{11} \\ \gamma_{22} \\ \gamma_{12}+\gamma_{21} \end{Bmatrix} + \begin{pmatrix} 0 & 0 & 0 & 0 \\ 0 & 0 & 0 & 0 \\ 0 & 0 & \dfrac{C^m_{11}-3C^m_{12}}{2} & 0 \\ 0 & 0 & 0 & \dfrac{C^m_{11}-3C^m_{12}}{2} \end{pmatrix} \begin{Bmatrix} \gamma_{11} \\ \gamma_{22} \\ \gamma_{12}-\gamma_{21} \\ \gamma_{21}-\gamma_{12} \end{Bmatrix} \tag{29b}$$

where the 3 independent constants are

$$C^m_{11} = \frac{l^2\rho^c}{8}\left(3K^m_n + K^m_s\right); \quad C^m_{12} = \frac{l^2\rho^c}{8}\left(K^m_n - K^m_s\right); \text{ and } C^m_{13} = \frac{-l^2\rho^c}{4}K^m_{ns} \tag{29c}$$

In the classical micropolar elastic model, only the 1st part of Eq. 26a, 27a and 29a, and the 2nd parts of Eqs. 26b, 27b and 29b survive where the antisymmetric $\sigma_{[ij]}$ is the eponymous micropolar stress (Germain, 1973). The antisymmetric term, $\gamma^{\phi}_{[ij]}$, can be written in terms of rotation (interpreted as micro-rotation in classical micropolar elasticity). Thus a part of the grain-pair relative displacement given by the micro-macro identification in Eq. 4, could be possibly interpreted as that contributed by grain rotations. It is noteworthy, however, that at the micro-scale, the deformation energy associated to the micro-rotation of micropolar elasticity is stored in the shear and shear-normal coupling between the grain-pairs as the grains displace. Indeed, it is not surprising that grain-scale mechanisms give rise to what appears as grain rotations from a macro-scale viewpoint. We particularly focus here on the shear and normal coupling terms in the grain-pair deformation energy in Eq. 13 (that is K_{ns}^{m}, where superscript α has been dropped since we consider here an averaged quantity). This shear-normal coupling at the grain-pair implies that the micro-structural and the mechanical principal axes of grain-pair interactions are not coincident. At macro-scale, this non-coincidence manifests as rotational degrees-of-freedom. Therefore, to model a beam (1D) composed of this material, it is necessary to introduce the coupling between the axial and rotational deformation (De Angelo et al., 2019a). In the 2D model derived here, the coupling component of the grain-scale deformation energy leads to the non-zero non-classical components that relate the symmetric part of the relative stress $\sigma_{(ij)}$ to the antisymmetric relative micro-gradient, $\gamma_{[ij]}^{\phi}$. Since the handedness of the local coordinate system (***n***, ***s***) determines the sign of the coupling stiffness, K_{ns}^{m}, a reflection transformation will change the sign of C_{13}^{m}, thus endowing the material with a chiral nature. Chirality in planar micro-polar elasticity has also been expounded through chiral lattice structures (see for example (Bahaloo and Li, 2019; Chen et al., 2014; Liu et al., 2012)) and also in 3D micro-polar elasticity through 3D lattices (Fernandez-Corbaton et al., 2019; Frenzel et al., 2017). Further, it could be interesting to examine and highlight chirality in the experimental observations in (Poncelet et al., 2018). It will also be interesting to investigate the chiral behavior of swarm robots, which also consider rather complex material particle interactions (Wiech et al., 2018).

Further, investigations are needed for unraveling the complex grain-scale mechanisms that give rise to higher-order or higher-gradient terms in the continuum models of granular systems. This is indeed the case if we consider that the grain displacements are coupled to grain rotations as introduced in (Misra and Poorsolhjouy, 2017; Poorsolhjouy and Misra, 2019) where the grain displacements are related to grain translation (rotation free) and grain spin (displacement free). The interrelationships between grain displacement, translation, rotation, and spin, in general, depends upon the complex micro-mechano-morphology of the granular material. For continuum modeling, however, the two fields of displacements, $\boldsymbol{\phi}$, and rotations, $\boldsymbol{\kappa}$, may be sufficient to describe the coupled kinematics of the material (Poorsolhjouy and Misra, 2019). It is also clear that the grain rotations can result in both normal and shear components of relative displacements for a grain-pair (Turco et al., 2019).

4. Experiments and Discrete Model Verification – the case of 1D Bead String

It is remarkable that the GMA predicts chirality in 2D granular media tied to the grain interactions. To verify these predictions, we have evaluated the behavior of a prototypical 1D granular material through independent numerical simulations and experimental method. A 1D bead string system was chosen over a 2D system due to the simplicity of the unitary granular string structure and the ability to experimentally characterize a 1D system. Different 2D structures and 3D structures will be synthesized and experimentally investigated in the future. It is also noteworthy that such a 1D system living in a 2D space does not possess centro-symmetry. Therefore, in this case, the terms that couple grain-pair relative rotations to the normal (axial) or shear (transverse) displacement could also have an effect. In other words, the continuum model for such a directed structure cannot be strictly isotropic belonging to symmetry class [SO(2)] and we could have coupling between the orders, such that the 5-th rank tensor has a role. In the present work, we highlight the effect pf coupling between grain-pair normal and shear displacements, and focus upon the chiral coupling discussed in the previous section. The effect of shear-normal-rotational coupling will be discussed briefly via a discrete model to indicate future possibilities. To this end, we have conceived a simple grain-pair interaction that exhibits shear-normal-rotational coupling. The grain-pair interaction behavior was computed using FE model in which each grain and grain-pair connection are treated as composed of classical Cauchy continua. This grain-pair interaction was then implemented into a 1D granular string and simulated using a discrete granular (DEM) model. The chiral nature was verified by evaluating the coupling between imposed axial loading and computed response in the transverse direction. Further, the 1D model results were validated with similar physical experiments on the exact geometry realized through 3D printing.

4.1 Grain-pair with coupled shear-normal-rotational interaction

Figure 2 shows the schematic representation of the conceived grain-pair interaction exhibiting shear-normal-rotational coupling. The set of solid bars and beams connecting two grains in Figure 2 may be considered as the mechanical (rheological) analog of grain-pair interactions. Such interactions can be possibly realized at the micro-scales through precision 3D printing or lithography(Ngo et al., 2018) or even through molecular or atomistic means using peptide engineering (Sarikaya et al., 2003). As a prototype of materials with such granular interactions that can be easily fabricated and realized through readily accessible technology, and one whose behavior can be precisely controlled within the sensitivities of the technology, we have directly implemented the designed analog. The geometrical parameters indicated in Figure 2(a) are provided in Table 1 for the fabricated system. The mechanical analog was analyzed using COMSOL, subjected to a series of boundary conditions to identify the grain-pair stiffness parameters in Eq. 13 (De Angelo et al., 2019a). An appropriate number of analyses by applying a combination of boundary condition indicated in Figure 2(b) were performed to identify all the grain-pair stiffnesses. The properties of the thermosetting printing material were assumed as follows: Young's modulus of 1.6 GPa and Poisson's ratio of 0.3. The resulting identified stiffness parameters are given in Table 2.

4.3 Experimental verification of Chirality in Bead String

A 3D computer generated model in CAD software SolidWorks (Dassault Systems SolidWorks Corporation, Waltham, MA, USA) was used to design the bead string geometry. This model has the dimensions reported in Table 1, and comprises 11 grains. The out of plane thickness of the system was taken as 4 mm. This value was chosen to be small enough to allow a 2D assumption, and large enough to prevent warpage of the sample in the fabrication process. Two small equally-sized cylinders (which we refer to as dots) were printed on each grain to facilitate the image processing used for tracking grain movements. The CAD model was printed using a Fused Deposition Modeling (FDM) Stratasys Mojo 3D printer using as constituent material an acrylonitrile butadiene styrene (ABS) thermoplastic material. An ElectroForce 3200 (TA Instruments) testing machine was used to conduct tensile test on the printed specimen. Figure 3 shows the experimental setup indicating also the clamped boundary conditions, such that on the top grain of the string a vertical displacement is applied while the lateral displacement is constrained, and on the bottom grain both vertical and lateral displacements are constrained. Figure 3(a) gives the initial (undeformed) configuration of one of the specimen, while Figure 3(b) shows the deformed configuration.

To track each grain, the following image processing approach was used. Dots on the left and right side of the grains were painted in black. A Nikon D700 camera was used to take consecutive pictures with fixed time intervals while the experiment was being performed with the sample set up in front of a red background to ease image processing. The black dots were identified and their centers of masses were labeled for each frame picture. The grain labelling was harmonized across all the images of the deformed configurations with the labels of the reference image using a minimum distance criterion test. This criterion works well especially when the deformation in successive frames is comparably small. Coordinates of grain centroids were calculated using the average of the coordinates of the black dots center of masses, with which grain centroid displacement was captured. The grain rotation for each grain in the structure can also be calculated by taking the vectors joining the dots at each time frame and using their inner product. The rotations of grains have not been presented in this paper as the resolution of the images and the experimental errors were comparable to the measurements of the rotations. Figures 4(a) through 4(f) give the results in terms of the grain vertical and lateral displacements, respectively, for the tensile tests performed on the three samples. It is remarkable that under an overall stretch of the 1D bead string, the grains undergo significant lateral displacements. Clearly, a reflection transformation about the vertical axis will change the sign of the lateral displacements indicating the chiral nature of the construct.

In Figures 4(a) and 4(b) the imposed displacement is 11.40 mm in vertical direction and the maximum lateral component of grain centroid displacement is measured as 0.34 mm. Similarly in Figures 4(c) and 4(d) the imposed vertical displacement is 12.03 mm and the measured maximum lateral component is 0.31 mm. Further, in Figures 4(e) and 4(f) the imposed vertical displacement is 11.50 mm and the measured maximum lateral component is 0.24 mm. It is notable that the 3D printed samples always have variability due to imperfections of the manufacturing process which introduces some randomness to the grain-pair interactions. The effect of randomness in grain-pair interactions is clear in the three experimental results shown in Figure 4. The variability is most noticeable in the nonzero lateral displacement the middle grain (as opposed to the prediction of DEM discussed in the next sub-section). We also note some nonzero lateral displacement for the clamped top grain in the first experiment. This is likely due imperfect clamping leading to grain slip in response to the lateral reaction that develops as expected in this type of media in which the axial (or normal) stretch is coupled to the lateral deformation. Similar chiral coupling between axial and transverse deformation at the macro-scale has been shown via a 1D beam model that includes additional degrees of freedom (De Angelo et al., 2019a). We believe, therefore, the observed behavior is characteristic of a micromorphic (or a more restrictive micropolar) model which includes internal degrees of freedom.

4.2 Discrete model for Chiral 1D granular material

To further verify the chiral behavior and explore the parametric space particularly with respect to effect of the strength of coupling between the modes of grain relative motions, a quasi-static discrete model of bead string was developed. For verification purposes, the discrete model considers 11 grains aligned vertically, with grain-pair interaction properties given in Table 2. Figure 5(a) shows a schematic picture of the 11-grain string system, where a 10% strain in vertical direction was imposed on the grain on top with the bottom-most grain completely constrained against displacements and rotations. Figure 5(b) and 5(c) give the vertical component and the lateral components, respectively, of the displacement of the grain centroids. The maximum vertical and horizontal component of displacement values for the imposed boundary conditions are computed as 11.5 mm and 0.28 mm, respectively. These values are in reasonable agreement with the experimental observations. Note that the scales of the vertical and horizontal components of displacements shown in Figure 5(b) and 5(c), have been adjusted for better visualization. Figure 5(d) shows the deformed configuration, where only the horizontal component of displacement has been scaled to accommodate visualization. As is seen from Figure 5(d), the rotation of grains is negligible. The maximum rotation is found to be 0.4 degrees. Figure 5(e) shows the energy distribution of grains, where maximum energy density is located in the center of the system.

It is worthwhile to note that the lateral displacements of the grains closest to the boundary grains are the largest which is also in agreement with the experiments. Indeed this aspect of the behavior can be modulated by controlling the strength of coupling of the grain rotations and the normal and shear displacements. In Figures 6 and 7, we show results for the case in which the coupling stiffness have been reduced to 50% and 10% of the values in Table 2. Interestingly, the location of grain undergoing the maximum lateral displacements shifts away from the boundaries as the coupling stiffness decreases. In addition, the deformation energy distribution appears to become more uniform. Further studies by varying the model parameters and using different boundary conditions can reveal additional variations of response and the effects of the grain-pair mechanisms. The proper continuum model that can capture these grain-scale mechanisms and replicate the macro-scale response may need to consider the complete micromorphic model of belonging to the appropriate symmetry class or anisotropy. These outstanding questions need to be pursued in future works.

5. Summary and conclusion

In the present paper, the granular micromechanics approach (GMA) has been applied to show that 2D granular systems exhibit chiral behavior at the macro-scale provided the grain-pair interactions are designed to have a coupling between relative displacements in the normal and tangential directions. Closed-form expressions for elastic constants of macro-scale 2D chiral granular metamaterial have been derived within the framework of micromorphic continua predicted by GMA. To verify the predicted chirality, 1D bead string model is conceived in which the designed grain-pair interactions have shear-normal-rotational coupling. This 1D bead string model was physically realized through additive manufacturing. The fabricated specimen were subjected to tensile experiment which showed lateral deflections. These experimental results were verified with discrete simulations for the 1D bead string in which grain-pair interactions mimic those in the physical specimen. Further, it was shown how the rotational-normal-tangential coupling stiffnesses (which are usually neglected in the literature when describing granular media) in grain-pair interactions alter the mechanical response and energy density concentration of the system for an applied load. It is clear that the GMA provides a systematic framework within which one can seek for grain-pair interactions that lead a desired mechanical behavior. By the same token, GMA can also be utilized to analyze a granular structure made of grains with particular (known) grain-pair interactions. Such capabilities make GMA applicable for the design and analysis of granular metamaterials when particular applications are sought after. Future studies are needed to further identify the grain-scale mechanisms and their effects at the macro-scale, such that the continuum models can be more strongly tied to the micro-scale mechanics.

Many mechanical metamaterials are designed with the intent to mitigate vibrations and demonstrate frequency bandgaps where a range of frequencies are filtered and not transmitted through the medium. In particular, granular metamaterials have an inherent length scale that promises dispersion. Model based upon GMA has shown dispersive behavior of granular media and has been utilized to analyze granular metamaterials for their wave propagation characteristics (Misra and Nejadsadeghi, 2019; Nejadsadeghi and Misra, 2019a; Nejadsadeghi et al., 2019b).

Along these lines, a dynamic response of the granular structure studied in the current paper will be analyzed using GMA and discrete simulation techniques in future publications.

Acknowledgements

This research is supported in part by the United States National Science Foundation grant CMMI -1727433.

References

Abdoul-Anziz, H., Seppecher, P., 2018. Strain gradient and generalized continua obtained by homogenizing frame lattices. Mathematics and mechanics of complex systems 6, 213-250.

Alibert, J.-J., Seppecher, P., Dell'Isola, F., 2003. Truss modular beams with deformation energy depending on higher displacement gradients. Mathematics and Mechanics of Solids 8, 51-73.

Altenbach, H., Eremeyev, V., 2014. Strain rate tensors and constitutive equations of inelastic micropolar materials. International Journal of Plasticity 63, 3-17.

Auffray, N., Dirrenberger, J., Rosi, G., 2015. A complete description of bi-dimensional anisotropic strain-gradient elasticity. International Journal of Solids and Structures 69, 195-206.

Bahaloo, H., Li, Y., 2019. Micropolar Modeling of Auxetic Chiral Lattices With Tunable Internal Rotation. Journal of Applied Mechanics 86, 041002.

Chen, Y., Liu, X., Hu, G., Sun, Q., Zheng, Q., 2014. Micropolar continuum modelling of bi-dimensional tetrachiral lattices. Proceedings of the Royal Society A: Mathematical, Physical and Engineering Sciences 470, 20130734.

De Angelo, M., Placidi, L., Nejadsadeghi, N., Misra, A., 2019a. Non-standard Timoshenko beam model for chiral metamaterial: identification of stiffness parameters. Mech Res Commun, 103462.

De Angelo, M., Spagnuolo, M., D'annibale, F., Pfaff, A., Hoschke, K., Misra, A., Dupuy, C., Peyre, P., Dirrenberger, J., Pawlikowski, M., 2019b. The macroscopic behavior of pantographic sheets depends mainly on their microstructure: experimental evidence and qualitative analysis of damage in metallic specimens. Continuum Mechanics and Thermodynamics 31, 1181-1203.

dell'Isola, F., Maier, G., Perego, U., Andreaus, U., Esposito, R., Forest, S., 2014. The complete works of Gabrio Piola: Volume I: Commented English Translation-English and Italian Edition. Springer International Publishing.

dell'Isola, F., Andreaus, U., Placidi, L., 2015. At the origins and in the vanguard of peridynamics, non-local and higher-gradient continuum mechanics: An underestimated and still topical contribution of Gabrio Piola. Mathematics and Mechanics of Solids 20, 887-928.

dell'Isola, F., Giorgio, I., Pawlikowski, M., Rizzi, N., 2016. Large deformations of planar extensible beams and pantographic lattices: heuristic homogenization, experimental and numerical examples of equilibrium, Proc. R. Soc. A. The Royal Society, p. 20150790.

dell'Isola, F., Seppecher, P., Alibert, J.J., Lekszycki, T., Grygoruk, R., Pawlikowski, M., Steigmann, D., Giorgio, I., Andreaus, U., Turco, E., Gołaszewski, M., Rizzi, N., Boutin, C., Eremeyev, V.A., Misra, A., Placidi, L., Barchiesi, E., Greco, L., Cuomo, M., Cazzani, A., Corte, A.D., Battista, A., Scerrato, D., Eremeeva, I.Z., Rahali, Y., Ganghoffer, J.-F., Müller, W., Ganzosch, G., Spagnuolo, M., Pfaff, A., Barcz, K., Hoschke, K., Neggers, J., Hild, F., 2018. Pantographic metamaterials: an example of mathematically driven design and of its technological challenges. Continuum Mechanics and Thermodynamics 31, 851-884.

dell'Isola, F., Seppecher, P., Spagnuolo, M., Barchiesi, E., Hild, F., Lekszycki, T., Giorgio, I., Placidi, L., Andreaus, U., Cuomo, M., ... 2019. Advances in pantographic structures: design, manufacturing, models, experiments and image analyses. Continuum Mechanics and Thermodynamics 31, 1231–1282.

Eremeyev, V.A., 2018. On the material symmetry group for micromorphic media with applications to granular materials. Mech Res Commun 94, 8-12.

Eringen, A., 1999. Microcontinuum Field Theories I: Foundations and Solids, 1999. Springer-Verlag, New York.

Eugster, S.R., dell'Isola, F., 2017. Exegesis of the Introduction and Sect. I from "Fundamentals of the Mechanics of Continua"** by E. Hellinger. ZAMM-Journal of Applied Mathematics and Mechanics/Zeitschrift für Angewandte Mathematik und Mechanik 97, 477-506.

Eugster, S.R., Dell'Isola, F., 2018a. Exegesis of Sect. II and III. A from "Fundamentals of the Mechanics of Continua" by E. Hellinger. ZAMM-Journal of Applied Mathematics and Mechanics/Zeitschrift für Angewandte Mathematik und Mechanik 98, 31-68.

Eugster, S.R., dell'Isola, F., 2018b. Exegesis of Sect. III. B from “Fundamentals of the Mechanics of Continua” by E. Hellinger. ZAMM-Journal of Applied Mathematics and Mechanics/Zeitschrift für Angewandte Mathematik und Mechanik 98, 69-105.

Fernandez-Corbaton, I., Rockstuhl, C., Ziemke, P., Gumbsch, P., Albiez, A., Schwaiger, R., Frenzel, T., Kadic, M., Wegener, M., 2019. New Twists of 3D Chiral Metamaterials. Advanced Materials 0, 1807742.

Frenzel, T., Kadic, M., Wegener, M., 2017. Three-dimensional mechanical metamaterials with a twist. Science 358, 1072-1074.

Germain, P., 1973. Method of Virtual Power in Continuum Mechanics .2. Microstructure. Siam Journal on Applied Mathematics 25, 556-575.

He, Q.-C., Zheng, Q.-S., 1996. On the symmetries of 2D elastic and hyperelastic tensors. Journal of elasticity 43, 203-225.

Liu, X., Huang, G., Hu, G., 2012. Chiral effect in plane isotropic micropolar elasticity and its application to chiral lattices. Journal of the Mechanics and Physics of Solids 60, 1907-1921.

Mindlin, R.D., 1964. Micro-Structure in Linear Elasticity. Archive for Rational Mechanics and Analysis 16, 51-78.

Misra, A., 1998. Particle kinematics in Sheared Rod Assemblies, Physics of Dry Granular Media. Springer, pp. 261-266.

Misra, A., Chang, C.S., 1993. Effective elastic moduli of heterogeneous granular solids. International Journal of Solids and Structures 30, 2547-2566.

Misra, A., Jiang, H., 1997. Measured kinematic fields in the biaxial shear of granular materials. Computers and Geotechnics 20, 267-285.

Misra, A., Lekszycki, T., Giorgio, I., Ganzosch, G., Müller, W.H., Dell'Isola, F., 2018a. Pantographic metamaterials show atypical Poynting effect reversal. Mech Res Commun 89, 6-10.

Misra, A., Nejadsadeghi, N., 2019. Longitudinal and transverse elastic waves in 1D granular materials modeled as micromorphic continua. Wave Motion 90, 175-195.

Misra, A., Placidi, L., Turco, E., 2018b. Variational Methods for Discrete Models of Granular Materials, in: Altenbach, H., Ochsner, A. (Eds.), Encyclopedia of Continuum Mechanics. Springer Verlag.

Misra, A., Placidi, L., Turco, E., 2019. Variational Methods for Continuum Models of Granular Materials, in: Altenbach, H., Ochsner, A. (Eds.), Encyclopedia of Continuum Mechanics. Springer-Verlag GmbH Germany.

Misra, A., Poorsolhjouy, P., 2015. Identification of higher-order elastic constants for grain assemblies based upon granular micromechanics. Mathematics and Mechanics of Complex Systems 3, 285-308.

Misra, A., Poorsolhjouy, P., 2016a. Elastic Behavior of 2D Grain Packing Modeled as Micromorphic Media Based on Granular Micromechanics. Journal of Engineering Mechanics 143, C4016005.

Misra, A., Poorsolhjouy, P., 2016b. Granular micromechanics based micromorphic model predicts frequency band gaps. Continuum Mechanics and Thermodynamics 28, 215-234.

Misra, A., Poorsolhjouy, P., 2016c. Granular micromechanics model of anisotropic elasticity derived from Gibbs potential. Acta Mechanica 227, 1393-1413.

Misra, A., Poorsolhjouy, P., 2017. Grain- and macro-scale kinematics for granular micromechanics based small deformation micromorphic continuum model. Mech Res Commun 81, 1-6.

Nejadsadeghi, N., De Angelo, M., Drobnicki, R., Lekszycki, T., dell'Isola, F., Misra, A., 2019a. Parametric Experimentation on Pantographic Unit Cells Reveals Local Extremum Configuration. Experimental Mechanics 59, 927-939.

Nejadsadeghi, N., Misra, A., 2019a. Axially moving materials with granular microstructure. International Journal of Mechanical Sciences 161, 105042.

Nejadsadeghi, N., Misra, A., 2019b. Extended granular micromechanics approach: a micromorphic theory of degree n. Mathematics and Mechanics of Solids (in print).

Nejadsadeghi, N., Placidi, L., Romeo, M., Misra, A., 2019b. Frequency Band Gaps in Dielectric Granular Metamaterials Modulated By Electric Field. Mech Res Commun 95, 96-103.

Ngo, T.D., Kashani, A., Imbalzano, G., Nguyen, K.T., Hui, D., 2018. Additive manufacturing (3D printing): A review of materials, methods, applications and challenges. Composites Part B: Engineering 143, 172-196.

Oliveira, A.R., 2017. D'Alembert: Between Newtonian Science and the Cartesian Inheritance. Advances in Historical Studies 6, 128-144.

Poncelet, M., Somera, A., Morel, C., Jailin, C., Auffray, N., 2018. An experimental evidence of the failure of Cauchy elasticity for the overall modeling of a non-centro-symmetric lattice under static loading. International Journal of Solids and Structures 147, 223-237.

Poorsolhjouy, P., Misra, A., 2019. Granular Micromechanics Based Continuum Model for Grain Rotations and Grain Rotation Waves. Journal of the Mechanics and Physics of Solids 129, 244-260.

Richefeu, V., Combe, G., Viggiani, G., 2012. An experimental assessment of displacement fluctuations in a 2D granular material subjected to shear. Geotechnique Letters 2, 113-118.

Sarikaya, M., Tamerler, C., Jen, A.K.-Y., Schulten, K., Baneyx, F., 2003. Molecular biomimetics: nanotechnology through biology. Nature materials 2, 577.

Seppecher, P., Alibert, J.-J., dell'Isola, F., 2011. Linear elastic trusses leading to continua with exotic mechanical interactions Journal of Physics: Conference Series 319, 012018.

Turco, E., dell'Isola, F., Misra, A., 2019. A nonlinear Lagrangian particle model for grains assemblies including grain relative rotations. International Journal for Numerical and Analytical Methods in Geomechanics 43, 1051-1079.

Wiech, J., Eremeyev, V.A., Giorgio, I., 2018. Virtual spring damper method for nonholonomic robotic swarm self-organization and leader following. Continuum Mechanics and Thermodynamics 30, 1091-1102.

List of Figures

List of Tables

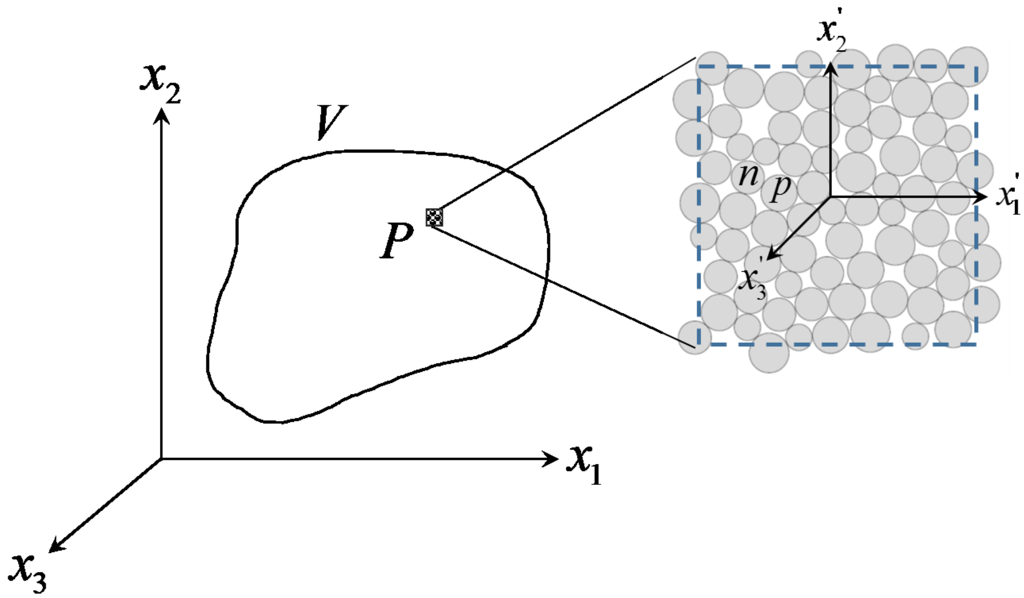

Figure 1. Schematic of the continuum material point, *P*, and its granular microstructure magnified for visualization, where the *x'* coordinate system is attached to its barycenter.

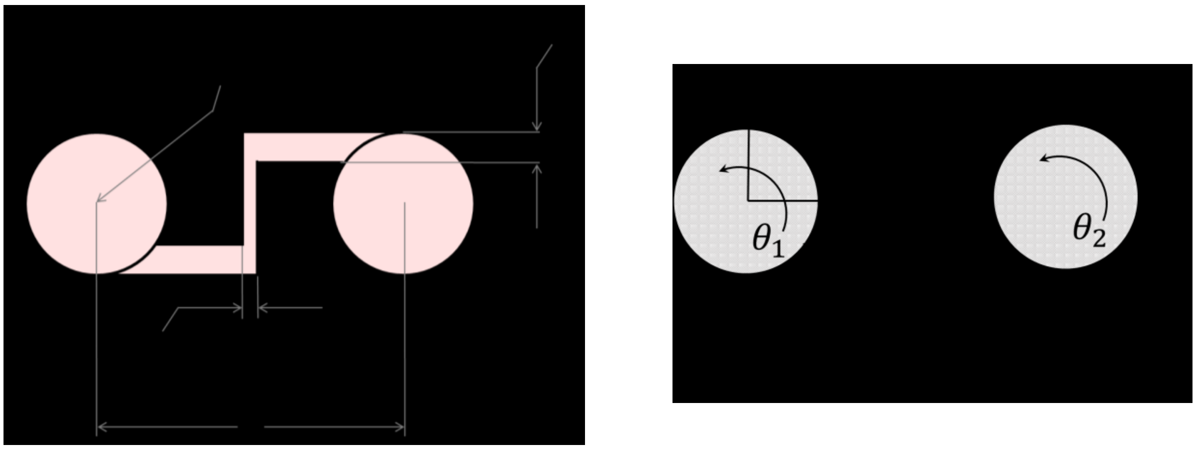

(a) (b)

Figure 2. A schematic representation of the grain-pair interaction possessing shear-normal-rotational coupling between grains: (a) dimensions of the mechanical analog, and (b) boundary conditions for determining the grain-pair stiffness constants.

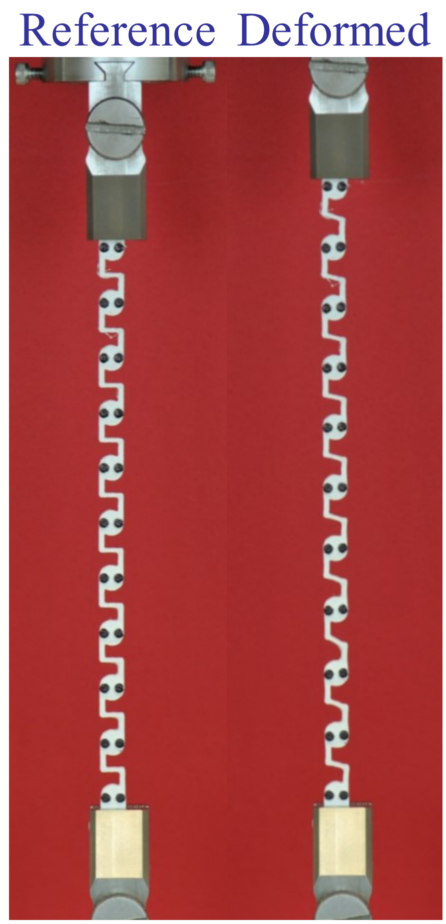

Figure 3. Experimental setup for testing the 1D bead string showing the reference and deformed configurations.

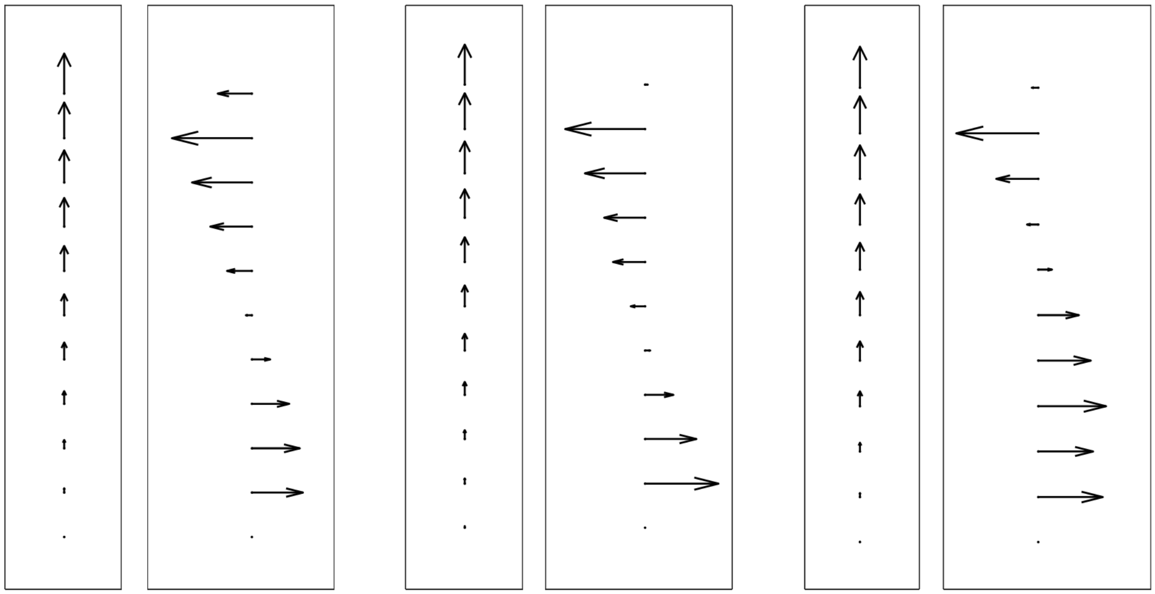

Figure 4. Experimental results for grain centroid displacements for 3 independent specimen: (a), (c) and (e) give the vertical components, and (b), (d) and (f) give the horizontal components of the grain centroid displacements.

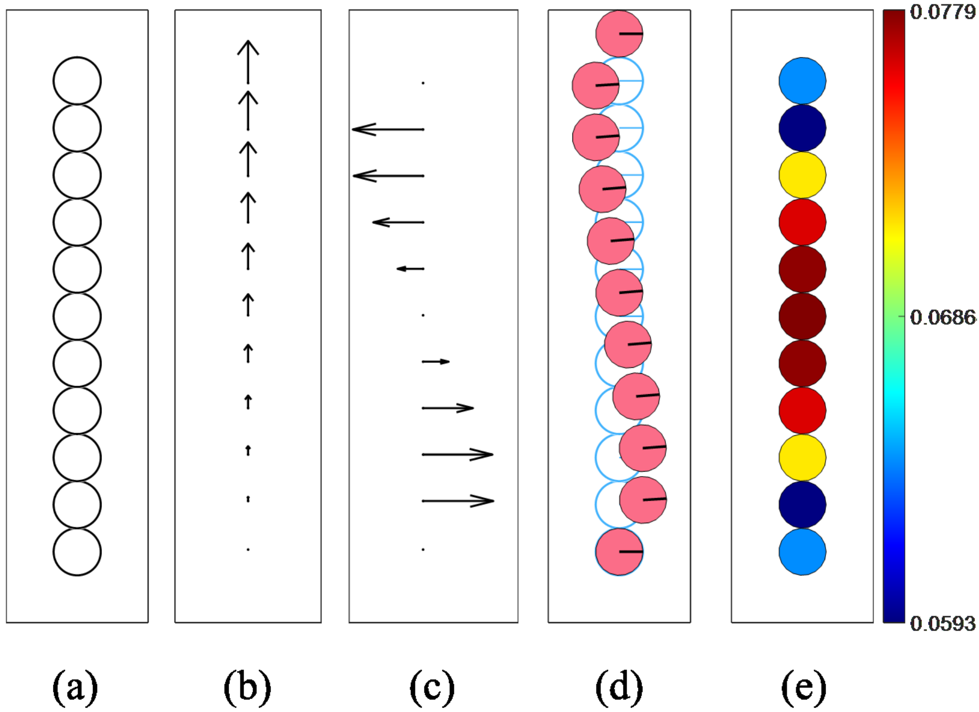

Figure 5. Discrete simulations of the 1D bead string. (a) A schematic representation of the 1D bead string. (b) Vertical component of displacement of grain centroids. (c) Horizontal component of displacement of grain centroids. (d) Deformed shape of 1D bead string. (e) Energy density distribution in the grains.

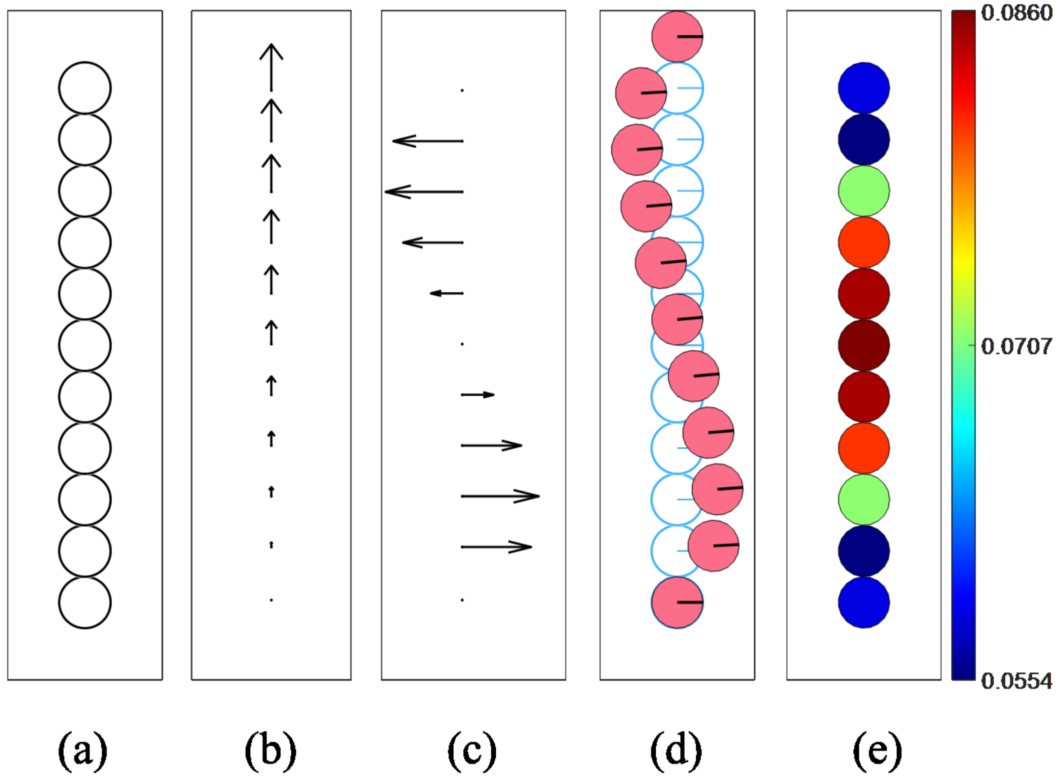

Figure 6. Discrete simulation of the 1D bead string with grain-pair interaction properties reported in Table 2, except for rotational-normal and rotational-shear coupling terms redefined as $D_n^{\alpha u}$ =36.39 N and $D_s^{\alpha u}$ =50.25 N. (a) A schematic representation of the 1D bead string. (b) Vertical component of displacement of grain centroids with maximum value of 11.5 mm. (c) Horizontal component of displacement of grain centroids with maximum value of 0.445 mm. (d) Deformed shape of 1D bead string (the horizontal component has been magnified by 20 times). (e) Energy density distribution in the grains

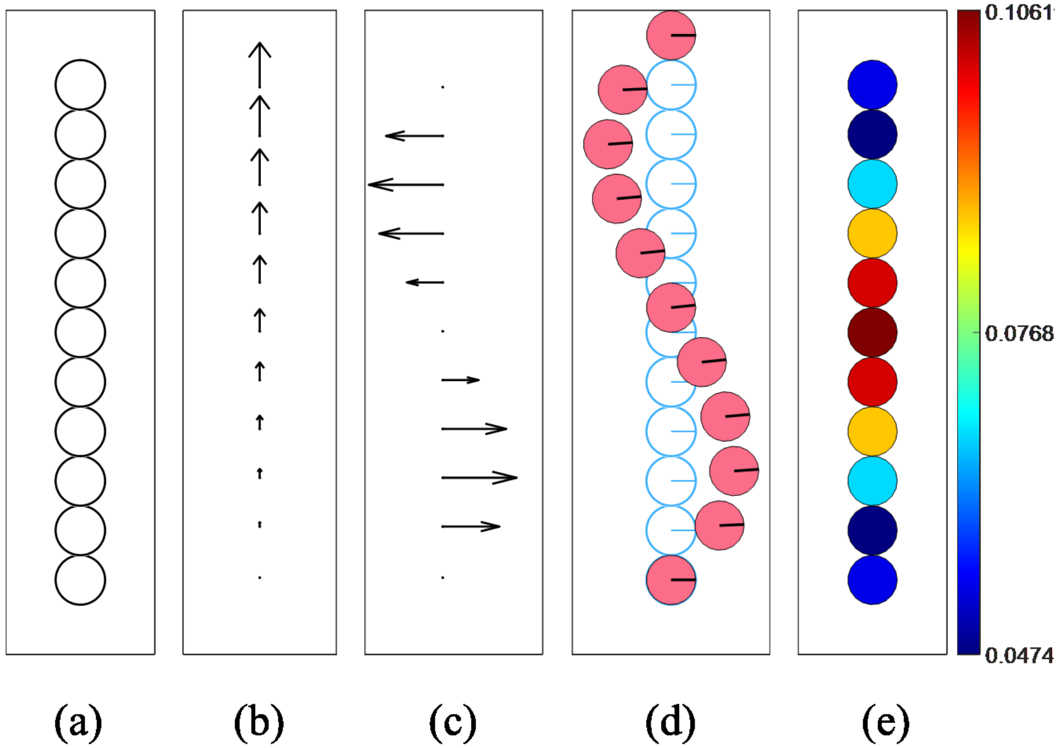

Figure 7. Discrete simulation of the 1D bead string with grain-pair interaction properties reported in Table 2, except for rotational-normal and rotational-shear coupling terms redefined as $D_n^{\alpha u}$ =3.64 N and $D_s^{\alpha u}$ =5.03 N. (a) A schematic representation of the 1D bead string. (b) Vertical component of displacement of grain centroids with maximum value of 11.5 mm. (c) Horizontal component of displacement of grain centroids with maximum value of 0.734 mm. (d) Deformed shape of 1D bead string (the horizontal component has been magnified by 20 times). (e) Energy density distribution in the grains.

Table 1. Geometrical parameters values corresponding to the proposed grain-pair interaction model

Model Parameter	Value
l	11.50 mm
r	2.65 mm
t	0.80 mm
b	1.15 mm

Table 2. Stiffness constants corresponding to the proposed grain-pair interaction model for DEM

Material Constant	Value
$K_n^{\alpha M} + K_n^{\alpha m}$	51.63 KN/m
$K_s^{\alpha M} + K_s^{\alpha m}$	52.44 KN/m
$K_{ns}^{\alpha m}$	37.98 KN/m
$G_3^{\alpha u}$	1.672 Nm
$D_n^{\alpha u}$	72.78 N
$D_s^{\alpha u}$	100.51 N